47th SME North American Manufacturing Research Conference, Penn State Behrend Erie, Pennsylvania, 2019

Illumination Compensated images for surface roughness evaluation using machine vision in grinding process

Jibin G. John[a], Arunachalam N[b]**

*a & b*Indian Institute of Technology Madras, Chennai-600036, India
*Corresponding author. Tel.: +91-44-2257-4722; E-mail address: chalam@iitm.ac.in

Abstract

Appropriate lighting is one of the indispensable elements in inspection using machine vision system. Illumination variation affects the accuracy and robustness of an inspection method that employs a machine vision system. The lighting inhomogeneity is the disturbing signal that needed to be suppressed to achieve accuracy and consistency in surface roughness quantification. In this work, the illumination compensation techniques are used for ground surface roughness evaluation by statistical texture parameters using machine vision method. The three-dimensional (3-D) surface roughness parameters are compared with the texture parameters. The experimental results are based on the ground surface images that are machined at different machining parameters. After the grinding process, the images are captured under halogen lighting. The acquired images of ground specimens are used for illumination compensation using: homomorphic filtering, Discrete Cosine Transform (DCT) based filtering and Fourier Transform (FT) based filtering techniques. This helps to suppress the low frequency components and amplify the high frequency components in order to extract the texture information. Owing the fact that the ground surfaces were weaker anisotropic surfaces, the second order statistical evaluation methods are used to extract the changes in the image texture due to the variation in surface roughness of the component. The texture parameters evaluated using these methods are correlated with the 3-D surface roughness parameters measured using an optical profiler. The texture parameters showed better correlation with the measured roughness values and this can be an integral part of any grinding system to inspect the machined components. In order to establish the homogeneity achieved after compensation of images, the inhomogeneity indicator and harmonic distortion values are calculated for the ground images.

Keywords; illumination compensation; texture parameter evaluation; machine vision; inhomogeneity evaluation; linear regression

1. Introduction

The surface topography plays a key role in defining the functional requirement of any machined component. The measurement and characterization of surface topography of machined surface is essential to control the manufacturing process and relate the parameters with functional requirement. Measurement can be classified based on the interaction with work piece as contact type and non-contact type measurement. In contact type, the measurement of manufactured surfaces is carried out by stylus based contact instruments [24]. The drawbacks of the stylus measurement are: (i) Small stylus radii that cannot penetrate into minute crevices. (ii) Sharp stylus tip

can damage the surface (iii) Low measuring speed. In current industrial practice, it is required to inspect each and every component machined out of the manufacturing shop floor to ensure the stringent surface tolerance requirements. The stylus based instrument may not be adequate to meet the requirement. With the advancements in optics, laser and high speed computational resources, there is a lot of opportunity to characterize the machined surface by non-contact methods: capacitance, pneumatic, ultrasonic, microwave, machine vision and optical method. Some of the non-contact characterization methods are discussed here. Abouelatta [1] proposed a method to measure the 3D roughness by combining a computer vision system with a light sectioning microscope. Dutta et al. [2]

calculated the surface roughness with variation in cutting time and tool wear examining texture descriptors of the turned surface images. The geometric search technique was utilized to find the optical surface roughness parameter value (Ga) of machined surface images and obtained the surface roughness of shaped, milled and grounded components by forming regression equation [3,4]. The surface roughness parameters were estimated based on the amplitude and spacing deviations in the gray level values, grey level peak values per unit length in grey level mages [5]. Ying-ho et al. [6] predicted surface roughness in turning process by computer vision using gray level surface images and adaptive neuro-fuzzy inference system. They compared the measured surface roughness value (R_a) with the features obtained from the images of machined processes in varied speed, feed and depth of cut. Kassim et al. [7] examined the fractal surface texture features of machined components using hidden Markov Model (HMM) to find the tool wear in turning and end milling operations. Lee et al. [8] measured surface roughness of turned components by a vision system and compared the gray level texture parameter with the stylus roughness value. Lee et al. [9] used adaptive neuro-fuzzy inference system to find surface roughness in turning operation and a demonstrated a relationship between average surface roughness values and texture characteristics of turned surface images. Narayanan et al. [10] estimated roughness of milled samples using a genetic algorithm hardware configuration to remove noise in the image. A correlation was obtained using both enhanced and raw image and the enhanced images showed better correlation with average surface roughness value, Ra. Palani and Natarajan [11] developed an artificial neural network (ANN) model based on back propagation method using image features obtained from 2D Fourier transform as inputs and surface roughness as output and predicted the surface roughness. Tomkiewicz [12] estimated the surface roughness value Ra of turned components with the help of the neural network. Gupta and Raman [13] designed a vision system to capture the scattered laser light from machined surfaces and different optical parameters were assessed. Damodarasamy and Raman [14] performed a comparison based study of gray level histograms collected from machined samples. Bradley [15] have utilized Hurst operator to calculate the fractal dimension and assessed surface texture of milled and ground surfaces. In the case of machine vision system, the images should be captured with higher stability in lighting to achieve uniform illumination to capture images. In the processing of images, there are a lot of difficulties and more processing time due to variation in brightness and intensity. It contributes to changes in texture pattern also. Pfeifer and Wiegers [16] described a method for adaptive control of imaging parameters to obtain an image that contains only the real edges. They eliminated the effects resulting from the specular reflection of the component for retrieving the the texture pattern more efficiently. Elango and Karunamoorthy [17] studied the effect of angle of illumination, the distance between the light source and the object and the machining direction on the optical parameters using the design of experiments. Freeling [18] described the design of proper lighting system based on the object shape and orientation for improved evaluation of surface defects in the finished surface.

Therefore, the previous works related to machine vision based inspection demands a downright evaluation for the illumination compensation of images in machine vision approach. Thereby, providing a detailed evaluation to quantify the surface texture parameters expeditiously. In this work, the surface topography of ground components is evaluated after illumination compensation technique using machine vision.

2. Experimental Details

In this experiment, High Carbon High Chromium (HCHC) Steel is used for the grinding operation to manufacture surfaces of varied surface finish. All the experiments were conducted on HCHC steel of dimension 30 mm x 20 mm. Grinding is performed under different machining parameters by changing the speed, feed and depth of cut. The machining parameters are tabulated in table 1.

Table 1. Grinding parameters

Machining parameters specifications			
Cutting speed (m/s)	21	24	27
Feed (mm/min)	5	10	15
Depth of Cut (µm)	10	30	50

2.1 Lighting Configuration and Image acquisition

A single point source halogen lamp is considered for illuminating the surface. The point source lighting is used to provide direct lighting to the specified location in the machined sample. The point source halogen light also has less intensity that helps to be appropriate for using it as a spot light for evaluating a specified location. Directional halogen light with wavelength in the range of 650nm to 700nm has been used for image acquisition at an angle of 45º. The spotlight diameter has been 2cm. The lighting setup is shown in Fig. 1.
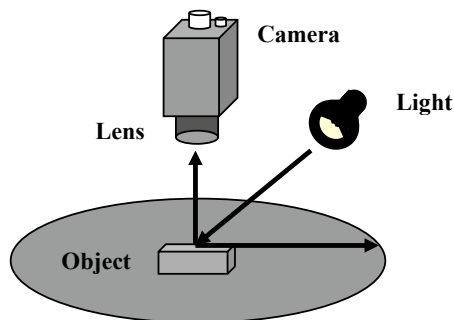

Fig. 1. Schematic of single point lighting system

The images were captured using Basler CCD camera of 1392 x 1040 resolution. The IEEE 1384 standard interface camera link at 17fps and C-mount for focus and aperture adjustment were used for image acquisition.

2.2 3-D Surface Roughness Measurement

The 3-D optical profiler was used for measuring the 3-D surface roughness (Bruker 3-D non-contact optical microscope) of the machined components. The components are scanned at a sampling length of 0.91μm to extract 3-D roughness parameters. The 3-D surface roughness parameters extracted are:

Average 3D surface roughness parameter, S_a,

$$S_a = \frac{1}{PQ}\sum_{R=0}^{P-1}\sum_{S=0}^{Q-1}[Z(x_r, y_s)] \qquad (1)$$

Root Mean Square (RMS) 3D roughness parameter, S_q,

$$S_q = \sqrt{\frac{1}{PQ}\sum_{R=0}^{P-1}\sum_{S=0}^{Q-1}[Z(x_r, y_s)]^2} \qquad (2)$$

Where, P & Q are number of data points in X & Y axis and Z (X_r, Y_s) is the amplitude variation. The 3-D surface roughness parameters are measured using the Bruker 3-D surface profiler at three distinct locations. The average 3-D surface roughness parameters (S_a & S_q) of grinding process are shown in Table 2.

Table 2. 3D surface roughness parameters of grinding processes.

Sl. No.	$S_a(\mu m)$	$S_q(\mu m)$
1	0.507	0.592
2	0.398	0.466
3	0.413	0.495
4	0.399	0.471
5	0.398	0.468
6	0.458	0.546
7	0.518	0.610
8	0.455	0.541
9	0.549	0.630
10	0.526	0.614
11	0.407	0.492
12	0.493	0.577
13	0.533	0.652
14	0.557	0.676
15	0.498	0.594
16	0.530	0.627
17	0.340	0.411
18	0.301	0.321

3. Illumination Compensation Method

The illumination affects the quality of the acquired images. The high-frequency components in an image are considered to be due to reflection and low-frequency components are presumed to be due to non-uniform illumination content in an image. Therefore, the high-frequency components are improved and low-frequency components are compressed to make homogenous luminance. The following illumination compensation methods utilized for image normalization.

3.1 Homomorphic Filtering

Homomorphic filter increases the contrast of the image and enhances reflective properties in an image. This technique discriminate the reflectance $R(u, v)$ and luminance $L(u, v)$ of image $I(u, v)$ by taking the natural logarithm and used for further normalization. The second stage is transforming the image to the frequency domain from the spatial domain using Fourier transform [19] .

$$F\{Z(u,v)\} = F\{\ln I(u,v)\} = F\{\ln R(u,v)\} + F\{\ln L(u,v)\} \qquad (3)$$

The image is filtered with the filter function *H(x,y)* that helps to amplify the high frequencies and lower the low frequencies. The normalized image *N'(u,v)* is finally obtained by finding the inverse Fourier transform of the filtered image and taking the exponential.

$$N'(u,v) = \exp\{F^{-1}[H(x,y).Z(x,y)]\} \qquad (4)$$

Where, $H(x, y)$ is homomorphic filtering function and $F\{Z(u,v)\} = Z(x,y) = F_R(x,y) + F_L(x,y)$. Normalized image *N'(u,v)* gives a high-frequency image with amplified high frequency and reduced low frequency.

3.2 Discrete Cosine Transform (DCT) Filtering

The DCT technique presumes that the illumination change is due to the low-frequency functions of the DCT transformed image. Thereby, discarding these low-frequency components and transforming the image by inverse DCT achieves the illumination invariance. Initially, the logarithm of the input image is taken to separate illuminance and reflection. The 2D-DCT of an image of $L \times M$ size is defined as [20] :

$$D(x,y) = \alpha(x)\alpha(y)\sum_{x,y} f(u,v) \times \cos[\frac{\pi(2u+1)}{2L}x]$$
$$\cos[\frac{\pi(2v+1)}{2M}y] \qquad (5)$$

And the inverse transform can be defined as

$$f(u,v) = \sum_{x=0}^{L-1}\sum_{y=0}^{M-1}\alpha(x)\alpha(y).D(x,y) \times \cos[\frac{\pi(2u+1)}{2L}x]$$
$$\cos[\frac{\pi(2v+1)}{2M}y] \qquad (6)$$

Where,

u & *v* are coordinates in image block, *L* x *M* in the spatial domain, *x* & *y* are coordinates in DCT coefficients, $\alpha(x)$ &

$\alpha(y)$ are basis functions of DCT, L x M is the size of image block.

$$\alpha(x) = \frac{1}{\sqrt{L}}, x = 0$$
, $\alpha(x) = \sqrt{\frac{2}{L}}, x = 1, 2, ..., L-1$,

$$\alpha(y) = \frac{1}{\sqrt{M}}, y = 0$$
, $\alpha(y) = \sqrt{\frac{2}{M}}, y = 1, 2, ..., M-1$

Now, low-frequency DCT coefficients are assigned to zero. Let, n be the number of DCT coefficients with values as zero. Then,

$$G'(u, v) = \sum_{x=0}^{L-1} \sum_{v=0}^{M-1} E(x, y) - \sum_{i=1}^{n} (x_i, y_i)$$

(7)

Where,

$$E(x, y) = \sum_{x=0}^{L-1} \sum_{y=0}^{M-1} \alpha(x)\alpha(y).D(x, y).\cos[\frac{\pi(2u+1)}{2L}x]$$

$$\cos[\frac{\pi(2v+1)}{2M}y]$$

Here the term $\sum_{i=1}^{n}(x_i, y_i)$ is considered as normalization term.

$G'(u, v)$ is the desired illumination compensated image.

3.3 Fourier Transform based filtering

The physical texture *t(u)* of the surface represented onto the gray level image during the image acquisition process helps in extraction of parameters. Texture *t(u)* and lighting inhomogeneity *i(u)* together forms the signal model for the textured surface image in the gray level domain. The inhomogeneity *i(u)* should be suppressed to enrich the texture information about the machined surfaces.

$$g(u) = i(u).t(u)$$

(8)

Where,

g(u) is the image captured by the CCD camera

t(u) is the texture and *i(u)* is the lighting inhomogeneity.

Beyer and Leon [21] separated the in-homogeneity signal *i(u)* into two spatially varying components $i_1(u)$ and $i_2(u)$. The $i_1(u)$

and $i_2(u)$ represents the local mean gray level value and the local contrast in the image respectively.

Then homogenization is done by

$$t(u) = H_2\{g(u)\} = \frac{g(u) - i_1(u)}{i_2(u)}$$

(9)

The varying component $i_1(u)$ subtracted from the image *g(u)* gives the first degree of homogenization and division of $i_2(u)$ gives the second moment of *g(u)*.

$$i_1(u) = LP\{g(u)\}$$

(10)

$$i_2(u) = \left(LP\left\{ \left[g(u) - i_1(u) \right]^2 \right\} \right)^{\frac{1}{2}}$$

(11)

where,

LP-is a Gaussian low pass filter

The homogenization is done using the Fourier transform and a Gaussian based low pass filter. The Fourier transformed image provides the local mean gray value and local contrast variation by subtracting the magnitude of compensated image from the original image. The local contrast $i_2(u)$ is extracted from Fourier transformed difference image by applying the Gaussian low pass filter. The final result is illumination compensated image after the Gaussian low pass filtering.

4. Illumination Inhomogeneity Evaluation

The variance in the illumination degrades texture pattern leading to loss of useful information in an image. These images are compensated using different illumination normalization techniques. The variation in illumination inhomogeneity of the images are analyzed by inhomogeneity indicator parameter and harmonic distortion proposed by Beyerer and Leon [21].

4.1 Inhomogeneity Indicator

The inhomogeneity value for the uncompensated and compensated images are compared to analyze the improvement in visual aspect of image. The image is separated in four equal parts and each part is further divided into four parts of equal window size to find inhomogeneity indicator. The process of partitioning is carried out as in Fig. 2.
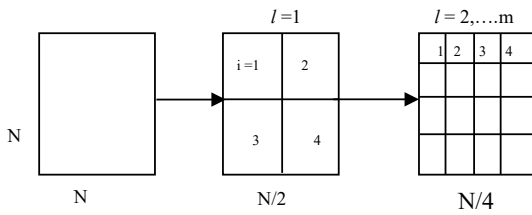
Fig. 2. Image segmentation for illumination inhomogeneity evaluation.

The cumulative histogram $H_{i,j}(g)$ is computed for each window, (i,j). The inhomogeneity indicator, Q_I for each window is calculated:

$$Q_I = \frac{1}{m} \sum_{i=1}^{m} \frac{2}{(4^l-1)4^l} \frac{1}{\sigma_l} \sum_{i=1}^{4^l-1} \sum_{j=i+1}^{4^l} d\left(H_{l,i}, H_{l,j}\right)$$

(12)

$$d\left(H_{l,i}, H_{l,j}\right) = \sum_{\gamma=g_1}^{g_G} |H_{l,i}(\gamma) - H_{l,j}(\gamma)|$$

Where,

The value of m must be selected such that the smallest windows of size, ($N/2^m$ x $N/2^m$) are larger than biggest details of the texture $t(x)$.

The mean empirical standard deviation σ_l in the plane, l is defined as:

$$\sigma_l = \frac{1}{4^l} \sum_{i=1}^{4^l} \left\{ \sum_{g=1}^{256} \left[g - \sum_{\lambda=1}^{256} \lambda h_{l,i}(\lambda) \right]^2 h_{l,i}(g) \right\}^{1/2}$$

(13)

The illumination inhomogeneity for the experimented lighting configuration and machining process are studied.

4.2 Harmonic Distortion

The harmonic distortion is mainly due to the nonlinear characteristics in any signal or image. The factor that has more effect on harmonic distortion is lighting. If the lighting is uniform, the harmonic distortion can be eliminated to a higher extent. In order to compare the harmonic distortion, the nonlinear characteristics are applied to a test signal of harmonic variations with a superimposed low frequency inhomogeneity in a particular bandwidth and a constant additive factor, μ. The harmonic distortion is determined by:

$$D = D\left\{H\left\{v(x)\right\}\right\} = \frac{\sqrt{(A_2^2 + A_3^2 + ...)}}{A_1} \quad (14)$$

The nonlinear distortion in a single image under different lighting is characterized using the harmonic distortion value.

5. Texture Parameter Extraction Methods

In machine vision system, the texture evaluation is based on the images captured. The images contain the useful information called texture which is the regular pattern in the surface of any object. In this context, the texture parameters are evaluated under the best lighting configuration for each process:

5.1 Gray Level Co-occurrence Matrix (GLCM) Method

A GLCM $p(k,l)$ is defined as a second order statistical matrix with all pairs of same gray level values and relationship between pixels within a region in an image. A GLCM is obtained for various directions 0˚, 45 ˚, 90 ˚, 135˚ for a distance (d), direction (θ) and gray level k x l [22]. From the obtained GLCM, selected second-order statistical parameters are extracted and the five parameters extracted are:

$$Contrast = \sum_{n=0}^{G} (n)^2 \left\{ \sum_{i,j} P(k,l) \right\}, n = |k-l|$$

(15)

$$Energy = \sum_{k,l} \left\{ p(k,l) \right\}^2$$

(16)

$$Entropy = \sum_{k,l} P(k,l) \log[p(k,l)]$$

(17)

$$Correlation = \sum_{k,l} \frac{\{k \times l\} \times \{p(k,l) - (\mu_u \times \mu_v)\}}{\sigma_u \times \sigma_v}$$

(18)

$$Homogeneity = \sum_{k,l} \frac{1}{1 + (k-l)^2} p(k,l)$$

(19)

Where,

$p(k,l)$: GLCM matrix of size $k \times l$.

n : Total number of gray levels.

μ_u & μ_v : Mean of p_u & p_v.

σ_u & σ_v : Standard deviations of p_u & p_v.

5.2 Gray Level Run Length Matrix (GLRLM) Method

GLRLM finds the pattern and direction of the gray level intensities and form a matrix to study the texture pattern. The gray level intensities in a definite direction, length and equal values constitute to form a run length. The run length matrix measures the recurrently occurring adjacent gray level values in a particular direction (0˚, 45 ˚, 90 ˚, 135˚). In different directions, run-length matrices are computed based on gray level values [23]. The following GLRLM texture parameters are extracted:

Short run emphasis,

$$SRE = \frac{1}{n}\sum_{k,l}\frac{p(k,l)}{l^2}$$

(20)

Long run emphasis,

$$LRE = \frac{1}{n}\sum_{k,l}k^2 p(k,l)$$

(21)

Run percentage,

$$RP = \sum_{k,l}\frac{n}{p(k,l)\,k}$$

(22)

Low gray level run emphasis,

$$LGRE = \frac{1}{n}\sum_{k,l}\frac{p(k,l)}{k^2}$$

(23)

High gray level run emphasis,

$$HGRE = \frac{1}{n}\sum_{k,l}k^2 p(k,l)$$

(24)

Where,

$p(k,l)$: GLRLM matrix of size $k \times l$.
n : Total number of gray levels.

6. Results and Discussions

The halogen lighting set up was used to capture the images of all the machined samples. The variation in intensity was studied with respect to halogen lighting in the grinding process and the samples showed better results under halogen lighting. The compensated and uncompensated ground images are shown in Fig. 3. The selected machined samples and respective GLCM and GLRLM parameters are tabulated in Table 3 and correlation coeffiecients are shown in Table 4.

Table 3. 3D surface roughness parameters and second order statistical texture parameters in halogen lighting of grinding process

| Sl. No. | 3D Surface roughness parameters | | GLCM Parameters | | | | | GLRLM parameters | | | | |
	Sa(μm)	Sq(μm)	Contrast	Corre-lation	Energy	Entropy	Homo-geneity	SRE	LRE	RP	LGRE	HGRE
Uncompensated Image												
Gr1	0.301	0.364	0.020	0.358	0.164	0.145	0.547	0.011	8.636	3.848	0.124	26.987
Gr2	0.493	0.577	0.206	0.643	0.315	1.292	0.855	0.074	14.237	8.009	0.229	102.18
Gr3	0.557	0.676	0.221	0.770	0.568	1.616	0.960	0.095	23.630	9.707	0.266	163.44
Homomorphic Filtering												
Gr1	0.301	0.364	0.028	0.425	0.029	0.507	0.575	0.046	30.120	3.588	0.144	12.166
Gr2	0.493	0.577	0.337	0.699	0.191	1.851	0.885	0.073	42.642	13.317	0.242	88.716
Gr3	0.557	0.676	0.627	0.837	0.360	2.585	1.030	0.067	47.628	18.752	0.300	192.11
DCT Filtering												
Gr1	0.301	0.364	0.289	0.490	0.089	1.449	0.510	0.008	11.867	8.673	0.051	27.037
Gr2	0.493	0.577	0.593	0.770	0.137	2.475	0.824	0.024	20.326	15.827	0.228	55.904
Gr3	0.557	0.676	0.573	0.895	0.162	2.723	0.939	0.033	27.387	17.532	0.345	77.614
FT Filtering												
Gr1	0.301	0.364	0.496	0.365	0.063	1.553	0.452	0.039	11.666	15.239	0.222	11.745
Gr2	0.493	0.577	0.908	0.590	0.101	2.623	0.741	0.064	19.677	24.739	0.358	19.866
Gr3	0.557	0.676	0.841	0.661	0.133	2.761	0.853	0.080	19.795	26.908	0.396	24.829
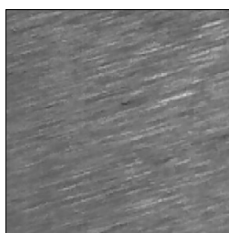
(a) Original image   (b) Homomorphic image   (c) DCT image   (d) FT image
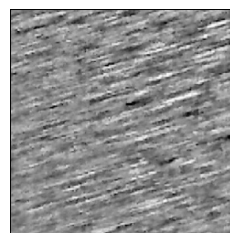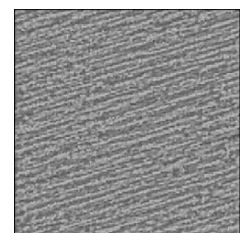
Fig. 3. Ground sample images under halogen lighting (S$_a$=0.493μm)

Table 4. Correlation between 3D surface roughness parameters, GLCM parameters GLRLM parameters of grinding.

| 3D surface roughness Parameters	GLCM Parameters					GLRLM parameters				
	Contrast	Correlation	Energy	Entropy	Homogeneity	SRE	LRE	RP	LGRE	HGRE
Uncompensated Image										
Sa(μm)	0.534	0.770	0.542	0.621	0.952	0.596	0.553	0.562	0.730	0.418
Sq(μm)	0.563	0.783	0.510	0.650	0.941	0.594	0.556	0.556	0.717	0.419
Homomorphic image										
Sa(μm)	0.615	0.965	0.557	0.700	0.969	0.649	0.681	0.709	0.843	0.500
Sq(μm)	0.607	0.953	0.552	0.699	0.948	0.644	0.669	0.706	0.833	0.496
DCT filtered										
Sa(μm)	0.723	0.970	0.786	0.977	0.995	0.787	0.729	0.917	0.974	0.741
Sq(μm)	0.719	0.962	0.784	0.964	0.985	0.784	0.718	0.902	0.978	0.749
FT filtered										
Sa(μm)	0.658	0.989	0.668	0.934	0.992	0.741	0.777	0.955	0.980	0.705
Sq(μm)	0.620	0.981	0.694	0.904	0.988	0.750	0.746	0.924	0.956	0.743
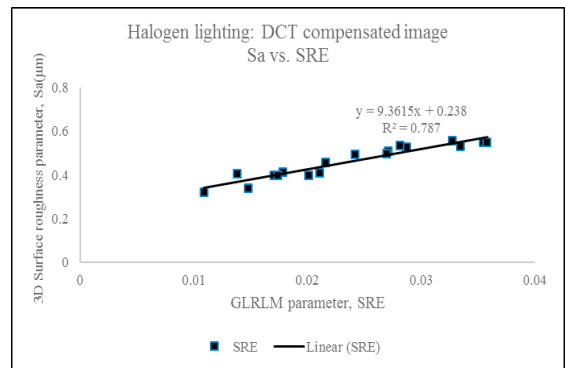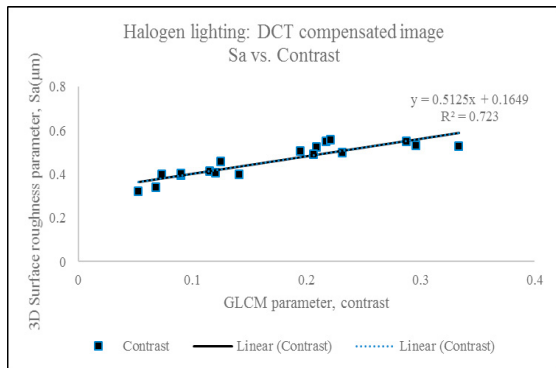
Fig. 4. Correlation of 3D surface roughness parameter, S_a with GLCM parameter Contrast and GLRLM parameter, SRE of DCT compensated images

The correlation was found to better in most of the texture parameters. However, contrast in GLCM parameter and SRE in GLRLM parameter are plotted in the Fig. 4 to show the correlation results. The inhomogeneity indicator and harmonic distortion values are evaluated for inhomogeneity evaluation and tabulated in Table 5. The inhomogeneity and linear distortion are reduced after the compensation of acquired ground images. However, the fourier transform and discrete cosine transform based compensation methods showed better inhomogenity and harmonic dostortion value.

Table 5. Inhomogeneity indicator and harmonic distortion values

	Inhomogeneity indicator value	Harmonic distortion value
Raw Image	0.320	10.98
Homomorphic compensated image	0.221	9.635
DCT compensated image	0.041	0.671
FT compensated image	0.062	0.670

Thus, it can be clearly infered that the illumination compensation techquies helps to improve the texture parameter quantification.

6.1 Validation of experimental results

The measured values of 3-D surface roughness values need to be validated with a set of data in grinding process. Thus, nine set of experiments are used for validation. The mean, standard deviation and coefficient of variance is found. The average 3-D surface roughness value, Sa is predicted using the equation obtained from the correlation model described in texture parameters extraction. The variation in lighting inhomogeneity under halogen light has been found based on the inhomogeneity indicator and harmonic distortion. The Mean, Standard Deviation and Coefficient of Variance are found as follows:

Mean, $\mu = \dfrac{\sum x}{n}$ (25)

Standard Deviation, $\sigma = \sqrt{\dfrac{\sum (x-\mu)^2}{n-1}}$ (26)

Coefficient of Variation, $C.O.V = \dfrac{\sigma}{\mu}$ (27)

Table 6. Actual and predicted surface roughness parameter.

Sl. No.	S_a actual(µm)	S_a predicted(µm): contrast	S_a predicted(µm): SRE
1	0.385	0.439	0.457
2	0.438	0.425	0.388
3	0.405	0.399	0.367
4	0.549	0.527	0.570
5	0.515	0.564	0.513
6	0.533	0.504	0.496
7	0.491	0.483	0.520
8	0.550	0.446	0.448
9	0.321	0.329	0.340
Mean	0.465	0.457	0.455
SD	0.082	0.071	0.077
C.O.V	0.176	0.155	0.169
Mean Squared Error (MSE)	0.045	0.050	

S_a predicted(µm)=0.5125 (contrast)+0.1649 (28)

S_a predicted(µm)=9.3615 (sre)+0.238 (29)

Finally, the 3-D surface roughness value (S_a) is predicted using contrast in GLCM and SRE in GLRLM texture parameters in grinding process as shown in Table 5. The correlation coefficient between the actual and predicted surface roughness value was found to be 0.677 and 0.620 with contrast and SRE as independent parameters respectively.
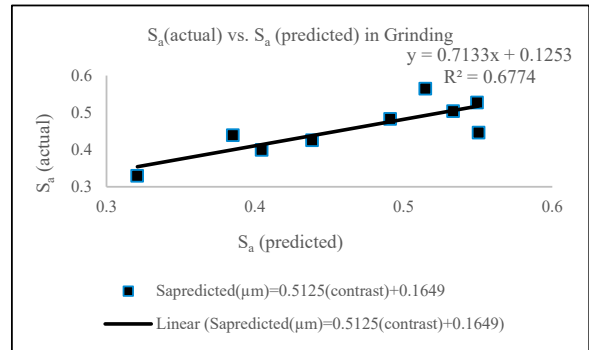

Fig. 5. Actual vs. predicted average 3D surface roughness value in grinding.

The 3-D surface roughness value predicted using the GLCM parameter, contrast in grinding process is shown in Fig. 5. The coefficient of variation of the predicted method is 0.155 and 0.169 using contrast and short run emphasis respectively. While, the actual roughness values showed a variation of 0.176. Thus, it is evident from the values of coefficient of variation that the predicted roughness values are showing less variation than the actual roughness values. The correlation coefficient of actual and predicted roughness can be improved if the size of training set is increased. This work is an initial step towards the research in the direction to estimate roughness using a comparison based faster approach that can be implemented in industries for higher productivity. Moreover, increase in training, testing and validation with multiple datasets could improve the results before practical implementation.

7. Conclusion

The surface characterization of ground surfaces can be analyzed using texture parameters. The illumination compensation technique proved to be effective in eliminating the inhomogeneity in different lighting configurations for different machining processes. The compensated images showed good correlation with 3D surface roughness parameters compared to uncompensated images. Therefore, it is eminent from the work that irregularities in illumination contribute to the texture pattern in an acquired image. The illumination compensated texture parameters showed better coefficient of correlation with the 3D surface roughness values in grinding process under halogen lighting. In this work, the second order statistical methods based on GLCM and GLRLM methods characterized the changes in the texture pattern of the images. The experimental results suggest an online measuring technique to control the surface quality of a machined part using these methods for a faster inspection in an industrial environment. This technique can be used as a comparator based

roughness estimation tool for faster inspection of surface roughness. Many other texture parameters can be used for texture based surface evaluation.

References

[1] O.B. Abouelatta, 3D surface roughness measurement using a light sectioning vision system, Proc. World Congr. Eng. 2010. WCE 2010. I 2010.p.6-11.

[2] A. Datta, S. Dutta, S.K. Pal, R. Sen, S. Mukhopadhyay, Texture Analysis of Turned Surface Images using Grey Level Co- occurrence Technique, 365 2012.p.38–43.

[3] B. Dhanasekar, B. Ramamoorthy, Restoration of blurred images for surface roughness evaluation using machine vision, Tribol. Int. 43 2010.p.268–276.

[4] R. Kumar, P. Kulashekar, B. Dhanasekar, B. Ramamoorthy, Application of digital image magnification for surface roughness evaluation using machine vision, Int. J. Mach. Tools Manuf. 45 2005.p.228–234.

[5] G.A. Al-kindi, R.M. Baul, K.F. Gill, An application of machine vision in the automated inspection of engineering surfaces, Int. J. Prod. Res. 30.1992.p.241–253.

[6] S.-Y. Ho, K.-C. Lee, S.-S. Chen, S.-J. Ho, Accurate modeling and prediction of surface roughness by computer vision in turning operations using an adaptive neuro-fuzzy inference system, Int. J. Mach. Tools Manuf. 42.2002.p.1441–1446.

[7] A.A.K. Zhu, M.M.A. Mannan, Tool condition classification using Hidden Markov Model based on fractal analysis of machined surface textures, Machine Vision and Applications. 17.2006.p.327–336.

[8] B.Y. Lee, H. Juan, S.F. Yu, A study of computer vision for measuring surface roughness in the turning process, Int. J. Adv. Manuf. Technol. 19.2002.p.295–301.

[9] K.-C. Lee, S.-J. Ho, S.-Y. Ho, Accurate estimation of surface roughness from texture features of the surface image using an adaptive neuro-fuzzy inference system, Precis. Eng. 29.2005.p.95–100.

[10] M.R. Narayanan, S. Gowri, M.M. Krishna, On Line Surface Roughness Measurement Using Image Processing and Machine Vision, Proceeding os the World Congress on Engineering. I.2007.p.5–7.

[11] S. Palani, U. Natarajan, Prediction of surface roughness in CNC end milling by machine vision system using artificial neural network based on 2D Fourier transform, Int. J. Adv. Manuf. Technol. 54.2011.p.1033–1042.

[12] A. Zawada-tomkiewicz, Estimation of surface roughness parameter based on machined surface image, Metrol. Meas. Syst. XVII.2010.p.493-504.

[13] M. Gupta, S. Raman, Machine vision assisted characterization of machined surfaces, Int. J. Prod. Res.7543. 39.2017.

[14] S. Damodarasamy, S. Raman, Texture analysis using computer vision, Comput. Ind. 16.1991.p25–34.

[15] S. Kurada, C. Bradley, A machine vision system for tool wear assessment, Tribol. Int. 30.1997.p.295–304.

[16] T. F, L. Wiegers, Adaptive Control for the Optimized Adjustment of Imaging Parameters for Surface Inspection Using Machine Vision, Annals of CIRP. 47.1998.p.487–490.

[17] V. Elango, L. Karunamoorthy, Effect of lighting conditions in the study of surface roughness by machine vision - An experimental design approach, Int. J. Adv. Manuf. Technol. 37.2008.p.92–103.

[18] R. Freeling, A. Arbor, The significance of industrial inspection tasks, Machine Vision International.1985.p.458–460.

[19] J. Short, J. Kittler, K. Messer, A comparison of photometric normalisation algorithms for face verification, Proc. - Sixth IEEE Int. Conf. Autom. Face Gesture Recognit.2004.p.254–259.

[20] W. Chen, M.J. Er, S. Wu, Transform in Logarithm Domain, 36.2006.p.458–466.

[21] J. Beyerer, Suppression of inhomogeneities in images of textured surfaces, Opt. Eng. 36.1997.p.85-93.

[22] R. Haralick, K. Shanmugan, I. Dinstein, Textural features for image classification, IEEE Trans. Syst. Man Cybern. 3.1973.p.610–621.

[23] M.M. Galloway, Texture analysis using gray level run lengths, Comput. Graph. Image Process. 4.1975.p.172–179.

[24] Whitehouse D. J., Surfaces and their measurment, Hermes Penton Ltd & Taylor Hobson Ltd.